A conceptual design in passive cooling and spray enhanced heat removal for spent fuel pool under severe accident threat

HUNG Tzu-chen[1], HSIEH Kai-ting[2], TSAO Po-chih[2], HUNG Michelle[3], TSENG Yung-shin[4], and CHEN Yitung[5]

1. Department of Mechanical Engineering, National Taipei University of Technology (NTUT), Taiwan (tchung@ntut.edu.tw)
2. Institute of Mechatronic Engineering, NTUT, Taiwan (g3u04jp6@livemail.tw)
3. Department of Biomedical Engineering, Cornell University, Ithaca, NY, USA (mh2233@cornell.edu)
4. Nuclear Science & Development Center, National Tsing-Hua University, Taiwan (yungshintseng@gmail.com)
5. Department of Mechanical Engineering, University of Nevada, Las Vegas, Nevada, USA (ychen@unlv.nevada.edu)

Abstract: The main purpose of this paper is to elevate the heat removal capability of spent fuel pool (SFP) and its safety for nuclear power plant. This research establishes a small-scaled device to perform numerical simulations and experiments to investigate its behavior after the nuclear accident. Firstly, to discuss if air would be the only medium for heat removal from spent fuel pool with the condition of no water existed. The research methods focus on using the combination of numerical simulation with experiments to explore the thermal-hydraulics phenomenon, and verify the numerical methods through experiments. Therefore, this study establishes a numerical model to perform the change in more difficult geometric parameter, and implement computer simulation to analyze its heat flow behavior. The result shows that the height of backplane, the numbers of aperture on backplane, the location of different watts of bundle rod heater, and the model geometry are the major causes of natural convection effect. In addition, cone spray nozzles were installed in the experimental apparatus to cool the heating rods. The coexistence of spray and natural convection resulted in an average of 5~15% improvement in temperature drop for the rods

Keyword: spent fuel pool; natural convection; spray experiments

1 Introduction

On March 11, 2011, Fukushima region in Japan experienced a 9.0 magnitude earthquake, which also caused tsunami that flooded the area. The Fukushima nuclear power plant was affected and experienced a loss of power; the reactor and SFP cooling system also experienced malfunction that lost its cooling ability. After Japan experience this dramatic incident, nuclear cooling method has been becoming an important topic of investigation performed by many different countries.

Alvarez *et al.* pointed out the SFP cooling water could fail in numerous ways for example, boil-off; they are drained into different volumes through the combination of valves, gates, and pipes that hold the water into the pool [1]. Wang *et al.* analyzed the performance of the SFP cooling system for Chinshan nuclear power plant (NPP) numerically. The result showed that fuel would occur in 2.7 days when undercover and around 3.5 days for metal water reaction after the cooling system failed. The effect of fire hydrant injection towards SFP was being analyzed as well. The results showed that the failure of cladding occurs in about 3.6 day if there is no fire hydrant water injection. However, the integrity of cladding is kept after the fire hydrant water injection [2-3].

The concept of natural convection application was widely known in people's daily life, for example, the chimney, ocean convection, and atmospheric convection are all natural convection effect. Dogan *et al.* used CFD software to design on a flat board device with different shaped upright flat board to investigate its natural convection. According to research, the fluid entrance surface area of the upright flat board would be the major influences of the natural convection. As the fluid pass by the upright flat board, it would be heated and then intersects with a low speed cold air to form a recirculating fluid space [4]. Hung *et al.* increased the holes on a computer motherboard, and the result showed that these holes have significant effects toward enhancing natural convection. This successfully elevated the

thermal dissipation efficiency on a PC board [5]. Yilmaz and Fraser once used single side of heat source to investigate the turbulent natural convection inside an upright flat board. As a result, the k-ε turbulent model in numerical simulation could accurately predict the model's average heat transfer rate and flow rate. The kinetic energy distribution between the flat boards indicates there is complete turbulent flow field around the exit [6]. Ng *et al.* investigated the pathway distance and natural convection turbulence model between the upright flat boards. The study concluded that the natural convection with vary width of flow path for the parallel upright boards could be describe as a mathematical speed model under certain circumstances [7]. This method is a useful reference towards further studies.

The safety of spent fuel is an important issue that has been the subject of many discussions. CFD software has been widely employed for the spent fuel application in recent years. Tseng *et al.* used the CFD software to execute simulations for a new type of tubular dry storage system. The results pointed out that the new storage design's thermal performance would meet the material structure and temperature requirement of NUREG-1536 [8, 9]. Ye *et al.* used the CFD simulation technology to perform a high efficacy heat pipe application towards the fuel pool with its passive heat removal capability. The fuel pool module was selected from the spent fuel pool of CAP1400 reactor, which is a passive pressurized water reactor modified from AP1000 [10]. The result was shown by using a fuel bundle that was placed for 15 years as the control group. The passive cooling system can effectively remove the decay heat and prevent the fuel rods from boiling. This result indicates that the passive cooling system could make water never boiled in a fuel pool even when experience the lack of external cooling system in an accident [11]. Yoo *et al.* used a scaled-down single fuel assembly to run the experiment and verify it with the CFD simulation. The result indicated that the result was similar between the experiment and the simulation. However, most of the parameters were in smaller scales except the temperature; the application might be inaccurate in real life situation and therefore it was not preserved nor quantized [12]. Hung *et al.*

completed the fuel pool's three-dimensional two-phase flow simulation by using CFD. The result indicated that the very crowded fuel configuration situation might cause local boiling on the fuel surface without auxiliary cooling system [13].

The spray nozzle application is widely known. Due to the high latent heat of liquid coolant, a great cooling effect would be utilized through the phase change of spray cooling in electronics, laser technology, and space technology [14]. Spray cooling was considered as one of the most promising techniques for high power thermal management by the advantages of high cooling efficiency, low flow rate, and the uniform cooling surface temperature distribution [15]. Jensen *et al.* studied different nozzle properties and the spray was affected by pressure, flow rate, height of the nozzles, and the type of valves [16].

Under the assumption of water loss of SFP and the expose of fuel bundles, this study proposed the concept of natural convection and sprinkler mechanism to enhance the security of the fuel pool. This study established a pool model to run the experiment and built a numerical model through CFD program at the mean time. Experiments and simulations were used for mutual authentication and expected to adjust the more difficult geometric parameters through CFD software to investigate the pros and cons of natural convection effect. Meanwhile, in order to conserve the limited water resources and to ensure the fuel pool cooling to reduce the temperature of the hot spots at the time of the accident, a concept of spray head sprinkler was used in the experiment and analysis in this study. Combined the concept with natural convection to intentionally receive better fuel pool safety and more rescue time when accident occurs. The concept of passive heat transfer is demonstrated in Fig. 1. Due to temperature caused density difference along the fuels, buoyancy force drives air flowing from the gap of the side channel, the bottom of fuel bundles, to the outflow of the internal tank. In order to effectively get more rescue time, the natural convection effect could strengthen by providing cool air towards the entrance. If this technique applies to the fuel pool of a nuclear power plant, then it could be a safe guard towards accidents.
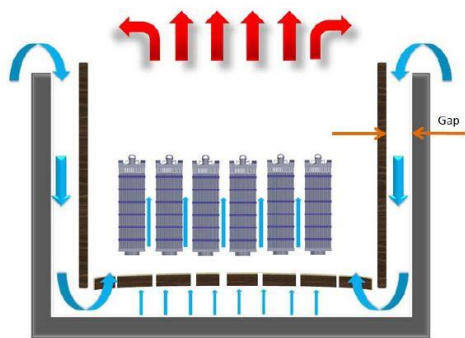
Fig. 1 Concept of passive heat removal for SFP.

2 Experiment setup

The purpose of this experiment is to investigate the natural convection and spray system towards the heat removal of SFP model. Experiment setup is shown in Figure 2(a).

2.1 Natural convection experiment

The natural convection experiment used a total of five bundles of heating rod and place in the SFP model in a line. As shown in Fig. 2(b), each bundle contains a 5x5 heating rods and placed them in the square shape pathway, and the design of the rod heater could be seen in Table 1. The power of the heating rod was controlled by SCR, and the power adjustments were shown on power monitor. This experiment used 3kW as the power for all five bundles of rod heater, and each rod contains 24 W. This value is evaluated based on the actual BWR. After removing away from the reactor core for a day, the decay heat would be approximately 12kW for a bundle containing 100 fuel rods. The heating length was 4m, which was 5 times longer than the active heating rod in the experimental model.

Table 1 Bundle rod heater

Item	Dimension
Rod heater	
Outer diameter	10mm
Length	1000mm
Pitch	13.5mm
Bundle	
Width	115mm
Length	1000mm
No. of rods	25 (5×5)
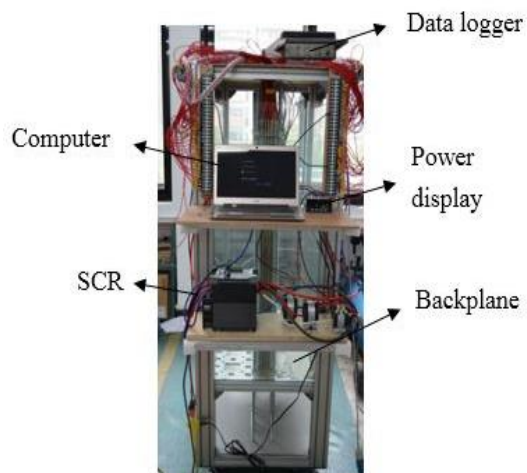
(a) Experiment facility
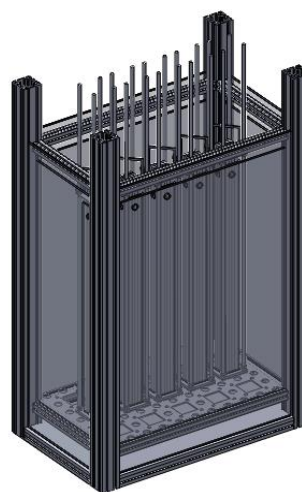
(b) SFP model

Fig. 2 A scale down SFP experiment installation.

The purpose of this study is mainly to compare the temperature distribution of different parameters. The parameters include the openings arrangement of backplane, the height of the backplane, forced convection, width of inlet air channel, *etc.* This paper mainly explores the effect of power of rod bundles, openings arrangement and height of backplanes. Three openings arrangements for the backplane are as shown in Fig. 3. The first arrangement, as shown in Fig. 3(a), has only one row of square holes for rod bundles open (Case 1). The second arrangement, as shown in Fig. 3(b), has all the round holes and three rows of square holes for rod bundles open (Case 2). Height of the backplane, as shown in Fig. 3(c), is set with H = 10 cm and H = 30 cm.

2.2 Spray experiment

Assuming the supply of SFP cooling pump was damaged or pipe fractured, it would cause the gradual decrease of SFP water level and the exposure of fuel. Once the cladding temperature is too high [17], this would cause the zirconium-water reaction. In a nuclear power plant, BWR fuel rod cladding normally operates between temperatures 270°C and 320°C. The spray head design was placed above the experiment model, so to lower the rate of accident and improve the heat dissipation of SFP. The spray head location is shown in Fig. 4, and there are a total of 8 sprays. Each was set with a height that is 20cm from the top of the rod heater, and the size of nozzle exit was 1mm. There are a total of 9 bundles of rod heater in the pool model. The air around them would be heated before spraying water and the buoyancy would occur and cause the driven of natural convection. When the rod heater reached up to 300°C, the cooling pump with then began to spray water. The circulation facility for the spray water is schematically shown in Fig. 5. After spraying for about 30 minutes, the rod heater temperature would no longer increase and the rod heater temperature distribution during water spray process was recorded.
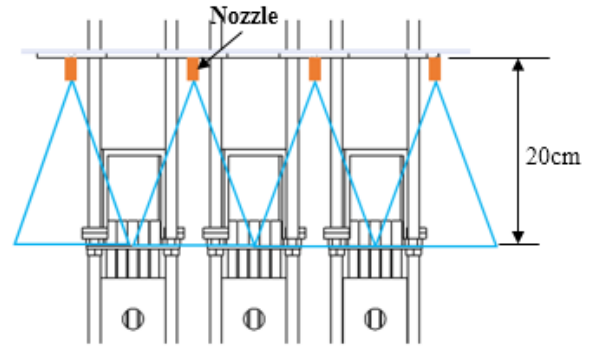

(a) Case 1   (b) Case 2

(c) Height of backplane

Fig. 3 Geometric parameters schematic.

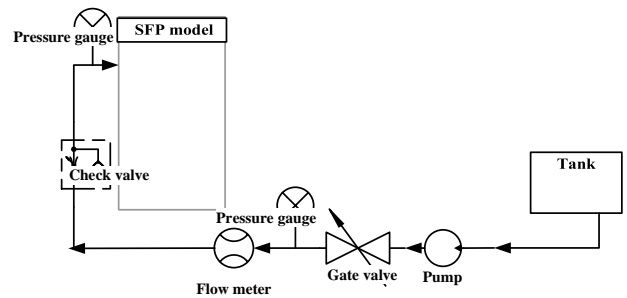Fig. 4 Spray installation schematic.

Fig. 5 Spray experiments schematic loop.

2.3 Installation of measuring instruments

In the experiments of natural convection without spray, the third bundle was installed with K-type thermocouples at rods 1, 7, and 13. The other 4 bundles were installed at rods 1 and 13, which was shown in Figs. 6(a) and 6(d). In the spray experiments, due to the lower temperature of rod heaters in the spraying process, each bundle of rod heater was installed with T-type thermocouples at rods 1, 7, and 13 as shown in Figs. 6(b) and 6(d).

The thermocouples were installed at the location of 10cm and 70 cm from the bottom of these rod heaters as shown in Figure 6(c). Before measuring, all thermocouples were calibrated. The following string of symbols represents the installation location of the thermocouples: for instance, "3-70cm-7", "3" represents the third bundle of rod heater as shown in Fig. 6(b); "70cm" represents the rod heater located at the height of 70cm from the bottom as shown in Fig. 6(c); "7" represents number 7 position of the rod heater as shown in Fig. 6(d). The measuring deviations of the K-type and T-type thermocouples were ranged ±1.1°C and ±0.5°C, respectively. For flow meter and pressure gauge, they were ±1% and ±2.5%, respectively.

The top view configuration of the heater bundles for the spray experiments is shown in Figure 6(b); the red part represents the location of spray head. This study selected different spray head set up compare to some existing nuclear power plants. The advantages of using spray head sprinkler was to spray more evenly compare to turret-type spray, and theoretically should make the fuel pool temperature decrease more evenly and reduce the occurrence possibility of hot spots. This could help saving more water resource in case accident happens. The required power consumption for pump and generator is expected to be less for spray head sprinkler compared to the turret-type sprinklers, so it has the advantages in both acquisition and delivery.
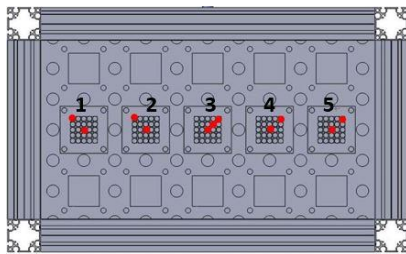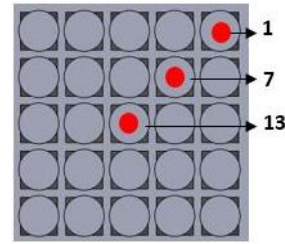
(a) Top view of Natural Convection Experiment
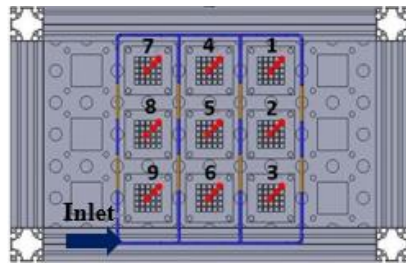
(b) Top view of Spray Experiment
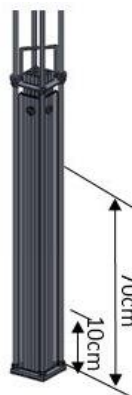
(c) Bundle rod heater isometric view

(d) Bundle rod heater top view

Fig. 6 Thermocouple installation schematic.

3 Mathematical modeling and numerical approach

3.1 Governing equations

Based on the descriptions mentioned above, the governing equations for the 3-D heat transfer problem with body force can be expressed as:

Continuity equation,

$$\frac{\partial \rho}{\partial t} + \nabla \cdot \left(\rho \vec{V} \right) = 0 \tag{1}$$

Momentum equations,

$$\frac{\partial}{\partial t} \left(\rho \vec{V} \right) + \nabla \cdot \left(\rho \vec{V} \vec{V} \right) = -\nabla p + \nabla \cdot \tilde{\tau} + \rho \vec{g} + \vec{S}_i \tag{2}$$

where, $\vec{V}\vec{V}$ represents the dynamic product:

$$\begin{bmatrix} uu & uv & uw \\ vu & vv & vw \\ wu & wv & ww \end{bmatrix} \tag{3}$$

and, $\tilde{\tau}$ represents the stress tensor:

$$\mu \left[\left(\nabla \vec{V} + \nabla \vec{V}^T \right) - \frac{2}{3} \nabla \cdot \vec{V} \tilde{I} \right] \tag{4}$$

For a homogenous porous media, the $\vec{S}_i$ term can be written as $\vec{S}_i = \left(\frac{\mu}{\alpha} u_i + K \frac{1}{2} \rho |V| u_i \right)$

Energy equation,

$$\frac{\partial}{\partial t} (\rho e) + \nabla \cdot \left[\vec{V} (\rho e + p) \right] = \nabla \cdot \left(k_{eff} \nabla T \right) + S_h \tag{5}$$

k_{eff} represents effective thermal conductivity, which includes both of molecular and turbulent conductivity:

$$k_{eff} = k + k_t \tag{6}$$

3.2 Thermal radiative effect

Considering the low natural convective flow in the ventilated-channel is the major heat removal mechanism, the radiation has comparable heat transfer rate and should be included in this simulation. At this temperature range, gas is not expected to participate in the radiation heat transfer. Radiation heat transfer mechanism can be simplified as a surface to surface radiation heat transfer problem.

The radiative heat flux between any two surfaces can be expressed by the equation developed by Incropera and DeWitt [18]:

$$q_{ij}^{''} = \sum_{j=1}^{N} A_i F_{ij} \sigma \left(T_i^4 - T_j^4 \right) \tag{7}$$

View factor (F_{ij}) can be written as:

$$F_{ij} = \frac{1}{A_i} \int_{A_i} \int_{A_j} \frac{\cos \theta_i \cos \theta_j}{\pi r^2} dA_j dA_i \tag{8}$$

But, the pre-calculation procedure for view factors requires large amount of CPU-time and storage-space. Thus, a precise and efficient radiative model is needed. Some numerical methods have been developed to improve the efficiency and accuracy of radiative heat transfer in complex geometries. Once way is to group the surface of similar temperature to reduce the total number of faces and the resulted view factors F_{ij}. However, it requires judgment and knowledge of finial temperature distribution. A finite volume method called Discrete Ordinary (DO) model has been employed to simulate radiation [19-21] and successfully applied to many complex geometries. Since the model with a symmetrical boundary condition and large mesh number was considered in this study, the DO model was employed to reduce the costs of pre-calculation and storage space for the radiative heat transfer treatment.

The DO model solves the radiation transfer equation to simulate the radiative transfer between cells, which can be written as

$$(\Omega \cdot \nabla) I(r, \Omega) = (a_{net} + \sigma_s) \left[I_b(r) - I(r, \Omega) \right] + \frac{\sigma_s}{4\pi} S(r, \Omega) \tag{9}$$

Generally, the absorption and scattering effects of gases at 1atm and the temperature of this problem are expected to be minimal.

3.3 Boundary conditions

The employed flow geometry with associate boundary conditions in this work is shown in Figure 7. The bottom surface of the computational domain is assumed to be an adiabatic surface. Furthermore, the inlet boundary condition is set at a uniform inlet temperature based on experimental ambient conditions (T_∞=21 ℃). For the other exterior surface of computational domain, a convective heat transfer combined with thermal radiation boundary condition was considered. The no-slip condition was applied to all solid-fluid interfaces to meet the fluid behavior. The heat flux balance at each fluid-solid interface can

be written as

$$q_{w,cond}^{''} = q_{w,conv}^{''} + q_{w,rad}^{''} \tag{10}$$

For the natural convection flow field, the buoyant force term is employed by Boussinesq approximation:

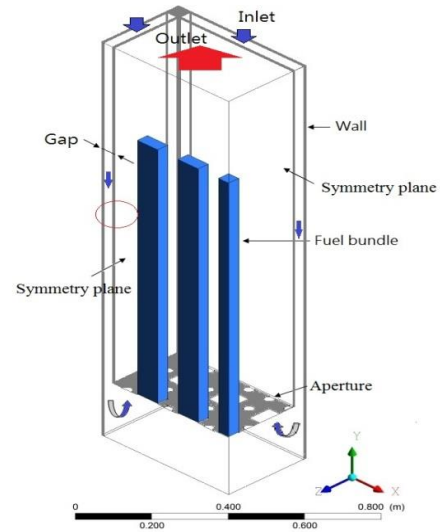$$\rho = \rho_0 (1 - \beta (T - T_\infty)) \tag{11}$$

Fig. 7 Boundary condition schematic.

3.4 Numerical treatment

The basic numerical scheme employed in this study is the Semi-Implicit Method for Pressure Linked Equations (SIMPLE) [22]. The finite volume approach [23, 24] was used to descritize the governing partial differential equations. The general form of the governing equations can be expressed as

$$\frac{\partial (\rho u_i \varphi)}{\partial x_i} = \frac{\partial}{\partial x_i} \left[\Gamma \frac{\partial \varphi}{\partial x_i} \right] + S_\varphi \tag{12}$$

All governing equations are integrated over each control volume (CV), leading to a set of algebraic equations for fluxes through CV surfaces and possible volumetric sources. All fluxes of each variable at cell faces are approximated based on the values of those variables at neighboring cell centers. The k-ε turbulent model [25] is employed to simulate the impact of the turbulent mechanism, and is governed by the equations of turbulence kinetic energy and turbulence kinetic energy dissipation.

The convergent residuals, for continuity and momentum equations need be converged to 10^{-3}, and for energy and radiation models need be converged to 10^{-6}. The form of residue in each equation can be expressed as:

$$R^\phi = \frac{\sum\limits_{cells-P} |\sum\limits_{nb} a_{nb}\phi_{nb} + b - a_p\phi_p |}{\sum\limits_{cells-P} | a_p\phi_p |} \qquad (13)$$

4 Results and discussion

4.1 Natural convection experiment

Figures 2(b) and 6(a) indicate the model for the experiment study herein with the circumstance of zero water existed in the pool. Since all heating bundles have the same heating power with symmetric layout, only bundles 3, 4 and 5 are discussed below. Two types of hole arrangement for the backplane were tested to compare which one is more efficient in passive heat removal by ambient air. As shown in Fig. 8(a), opening regions on the backplane are those in white. Case A1 only allows the air flowing through the openings beneath the heating rods; case A2 allows the air to flow through all openings. Though it is expected all the effective air to cool the heating rods, the temperatures of the rod 13 indicate that Case A1 has higher average temperature than Case A2 for all bundles. It is attributed to that the heating rods with electrical wires and thermocouples result in a great flow resistance to restrict the buoyancy driven downflow along the side gap. The temperature between two cases can be obviously seen.

The influence of backplane height to the temperature distribution is shown in Figure 8(b). Since smaller space beneath the backplane cause greater flow resistance for cold air flowing through the heating bundles, the height of 10cm results in a higher rod temperature than that of 30cm. The central bundle has relatively highest temperature distribution but the bundle 4 has the lowest. The result implies that small height of backplane causes a non-uniform flow upward flow field. The one of H=30cm produces a more uniform upward flow distribution and hence uniform temperature. The maximum magnitude drop of temperature distribution for rod 13 (the central rod in Fig. 6(d)) could be about 55°C.
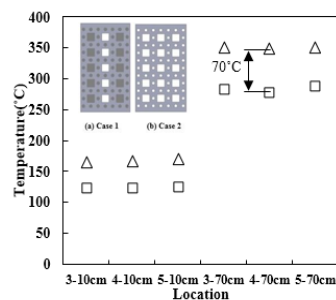
(a) Effect of backplane hole arrangement on temperature at H=30cm
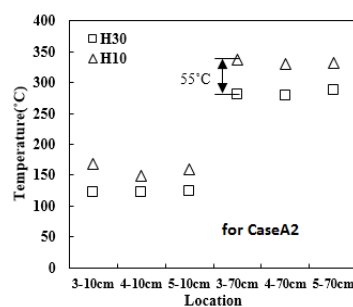
(b) The temperature comparison for various backplane height

Fig. 8 Comparison of temperature under natural convection for rod 13 (Δ caseA1; □ caseA2).

4.2 Experiment and simulation verification

The resulting comparison of CFD simlation and experiment with different open-hole methods and with different backplane height are shown in Figure 9. The 5 bundle rod heaters as shown in Fig. 6(a) are used as the heat source control group. The figure only points out the more interesting and important points as the main focus of this study. The temperature from CFD simulation is lower than the experimental measurement. This is because the experiment measurement thermocouples were located on the surface of the rod heater, but simulation measurements were located at the point of fluid inside the porous region. Meanwhile, there are many wires on top of the laboratory equipment for the purpose of electrical heating to the rod heaters, that increased the flow resistance and therefore caused the rise in temperature. Altough the error between the simulation and experiment was between 7% to 25%, the temperature distributions were similar. Since this study focused on investigating the temperature distribution and the effect of flow field inside the model, the CFD model and simulation technique should be reliable.
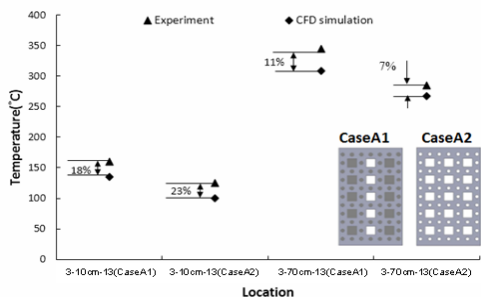
(a)　The arrangement of backplane flow path
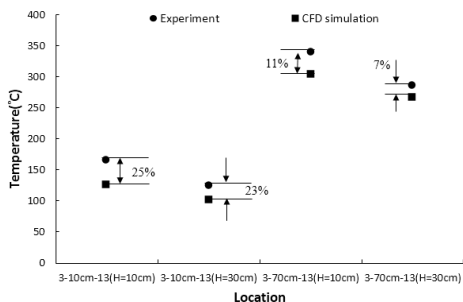
(b) The change of backplane height for CaseA1

Fig. 9 Comparison between experiment and simulation,

$$\left(\frac{T_h - T_l}{T_h - T_\infty}\right).$$

## 4.3 CFD investigation for wattage arrangement of heating bundles

4.3.1 Three dimensional simulations

A three-dimensional 5x5 rod bundle CFD simulation has been implemented to obtain the relationship of pressure drop of air against velocity through the porous component by Tsao *et al.* [26]. The inertial resistance and the permeability for the source term of momentum equation were determined; they are $C_2 = -2.966$ 1/m and $\alpha = -6.93 \times 10^{-7}$ m^2, respectively. Fig. 10(a) shows the top view of a 15-bundle rod heaters for three-dimensional CFD simulation model. For symmetrical reason, the arrow point direction represents the one-fourth area of pool was used in simulation. This study used a fuel rod contains two different Watt of rod heaters, 24W and 12W, for the purpose of analyzing their influence in passive heat removal. The 24W rod heater bundles were placed at the bundle of rod heater in CaseB1 at 1, 4, 5, and 6 and in CaseB2 at 2, 4, and 6. The 12W rod heater bundles were placed in CaseB1 at 2 and 3 and in CaseB2 at 1, 3, 5. In accordance with common sense, the arrangement of rod heater bundle in CaseB1 should cause higher temperature due to its excessive concentration of cavity heat source in the central region of the pool. Even so, this study selected the

arrangement from CaseB1 in order to increase the bouyancy, so that air would flow more smoothly from the bottom of the cavity to make its ascent. The flow field of this study was designed such that air would enter into the cavity, traveling to the base of the flatboard, and majority of the air would merge at the core of the base of flat board and then ascend. The middle flow path of the rod heater bundle will be expected to have the greatest flow rate. By placing the higher power density rods in the middle of the cavity flow path might cause stronger bouyancy, and enhance the flow rate to strengthen and speed up its heat dissipation. The simulation result shows that the speculation was reasonable. Figure 10(b) showed the cross-sectional average temperature comparison between CaseB1 and CaseB2; the cross-section were located at the height of 0.35m, 0.65m, 0.95m, and 1.25m. The graph indicated that the average temperature of CaseB1 was not higher but lower than CaseB2.
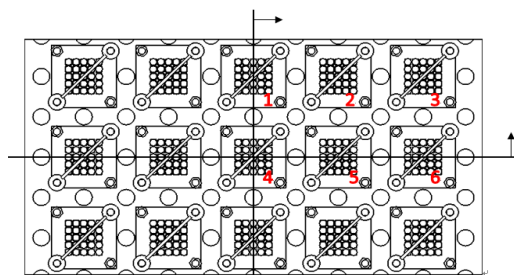
(a)　The schematic of rod heater bundle identification number
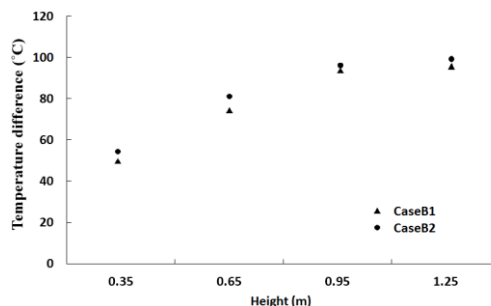
(b)　Cross-sectional average temperature rise for CaseB1 and CaseB2

Fig. 10 The result of different wattage arrangements.

The comparative data are shown in Table 2. The outlet flow is slightly higher for CaseB1 comparing to CaseB2, but the average temperature of the cavity and its high wattage rod heater bundle are higher for CaseB2 compared to CaseB1; low wattage rod heater bundles have the same temperature. In terms of the flow rate, high-wattage bundle appear to be higher for CaseB1 compared to CaseB2, but the low wattage

portion has almost the same flow speed. The highest local speed inside the bundle is approximately 0.5 m/s higher for CaseB1 compared to CaseB2, which is worthy to be mentioned. This was a pivotal speed in natrual convection. Therefore, we could determine that the arrangement of rod heater bundle in CaseB1 could induce a higher efficiency in natural convection.

Table 2. The comparison result of different Watts rod heater bundle arrangement

	Exit flow rate (m³/s)	Cavity's average temp. (°C)	24W bundle average temp. rise (°C)	12W bundle average temp. rise (°C)	24W bundle average velocity (m/s)	12W bundle average velocity (m/s)	Max. local velocity (m/s)
CaseB1	0.018	90	175.6	139.7	1.5	0.96	3
CaseB2	0.017	94	180.5	139.6	1.4	1.00	2.5

4.3.2 Two dimensional simulations

A series of two-dimensional simulations, which employed the bundle layout as that shown in Figure 6(a), have been implemented. The rod wattage distribution for the bundles from center to the side of the pool model in CaseC1 were 24W, 16W, and 8W; CaseC2 were 8W, 16W, and 24W. The main purpose of this study is to investigate if differential wattage of heating bundle configuration would produce an apparent effect on natural convection, while the sum of the rod heater bundle wattages were the same in the fuel pool model.

The comparison graph of temperature distribution for two-dimensional with two different wattage arrangement is shown in Figure 11. Due to the effect in natural convection, the different wattage arrangement would cause the temperature field inside the model to have direct impact on air bouyancy for each bundle. Between these two wattage configurations, the simulation result clearly shows that the temperature distribution is significantly decreased for CaseC1. It is known that when rod heater bundle wattages were the same, the flow rate at the center of rod heater bundle would be the fastest. This study was based on this phenomenon and it purposely strengthen the smoothness of the natrual convection by arranging the wattages accordingly to approach the best cooling effect. The rod heater bundle arrangements in CaseC2 could

cause internal conflict with this study. Table 3 is used to compare the performance between CaseC1 and CaseC2 via the cavity's average temperature, buoyancy induced exit flow rate, the average temperature and the highest flow rate inside the heater bundle. The average temperature of the cavity and for each heater bundle are higher for CaseC2 compare to CaseC1, but the flow rate is lower in CaseC2 than CaseC1. The data indicate better natural convection for CaseC1 compare to CaseC2, which reemphasizes that the different rod heater bundle wattages and arrangements would greatly effect the temperature distribution inside the cavity.

4.4 CFD investigation for pool geometry beneath the backplane

Here, the study would focuses on the change of geometric shapes of the ground and the backplane within the pool model, and explores its impact on the natrual covection effect when the water is completely lost. As shown in Fig. 12, the temperature distribution was given by the simulation of four types of gemetric parameters. The relative temperature was based on the color bar on the left, and it is clear that the overall temperature for CaseD1 is the lowest out of all four types of geometry. According to previous research, it was significantly helpful to increase the smoothness of airflow for natural convection effect. The purpose was to guide the airflow into the cavticy by chaning the geometric parameter. Bouyancy is an important parameter for natural convection studies, therefore, the density gradient in the flow path was used for comparison. After the comparison, the cooling effect was shown to be better for the original model (Base case) compare to CaseD2 and CaseD3.

Table 3. Two-dimensional simulation result with different wattage arrangements

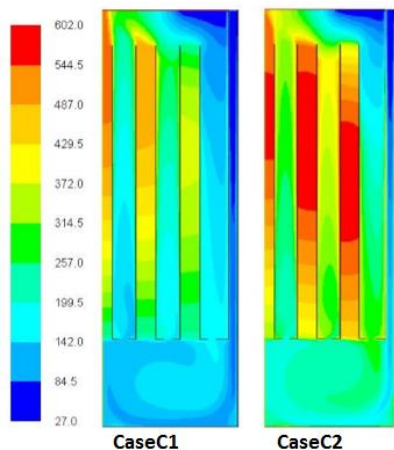|	Exit flow rate (m³/s)	Cavity's average temp. rise (°C)	Average temp. rise in 24W bundle (°C)	Average temp. rise in 16W bundle (°C)	Average temp. rise in 8W bundle (°C)	Rod heater bundle's max. flow rate (m/s)
CaseC1	0.065	163.7	419.8	388.1	305.7	1.26
CaseC2	0.059	268.4	513.8	482.5	481.7	1.01

Fig. 11 Temperature distribution comparison for different wattage arrangements.

Therefore, Base case is compared with CaseD1 individually. Figure 13 indicates the fluid velocity distribution along flow paths A and B between CaseD1 and the original model (Base case). The figure indicates that the flow rate close to the bottom of the rod heater bundle was relatively higher, because the holes would shrink while the fluid pass by its base flow path and would cause the increase in flow rate. As the flow path widen, flow rate will then decrease. The flow velocity along path B is about the same for CaseD1 and the original model, but with significant difference for flow path A; because CaseD1 model geometry could reduce the flow resistance and help guiding the air flow more smoothly.
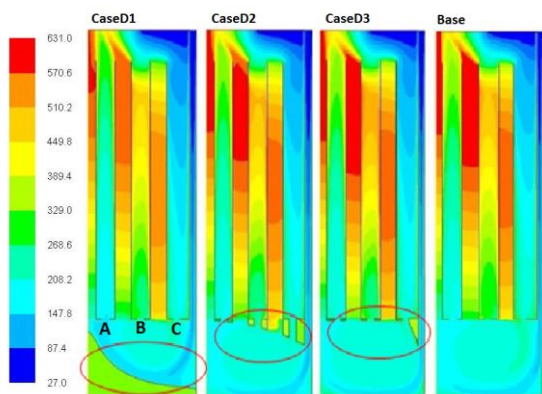

Fig. 12 Temperature distribution for different geometretic model.

4.5 Spray experiment

In the nuclear power plants, water resources are relatively precious. When the accident happened, assuming the SFP cooling system is damaged, causing real internal SFP water evaporation and loss. Under such circumstance, the pump would be unable

to provide the necessary cooling water in time to cover all the spent fuel rods to maintain their integrity. A major advantage using the sprinkling system is that it can sprinkle on top of the SFP so that it can provide quick thermal dissipation on the top part of the fuel bundle where higher temperature exists. Therefore the fuel will not break to prevent occurring greater disaster.
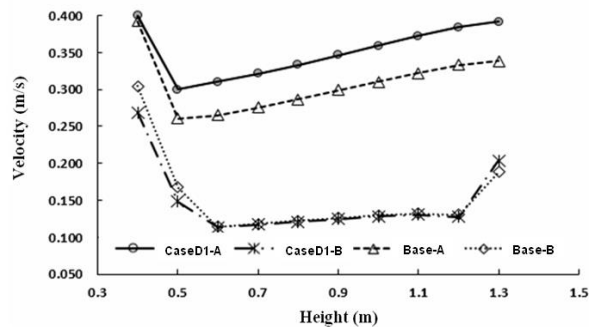

Fig. 13 Velocity comparison between CaseD1 and Base case.

In the SFP model, the main purpose of the experiment is to use the minimal amount of sprinkling water to achieve optimal thermal dissipation, allowing the temperature of the heating rods to be maintained at or below 300°C in order to prevent the occurrence of zirconium-water reaction. This experiment would simultaneously explore natural convection and water sprinkling in order to discuss how natural convection enhanced the thermal dissipating capability of the water sprinkling. In the following figure, natural conduction was studied under each case of water sprinkling. According to Figs. 14(a) and (b), it is obvious that thermal dissipation was enhanced when there is natural convection as opposed to without it. This is likely because the steam rise very quickly in the water sprinkle experiment. In the case of closing the side flow channels (defined as the "No NC" in Fig. 14) of the pool cavity, the heated air will not be able to smoothly flow out of the upper exit. The cold air is not able to supply the SFP model from the side channels of the cavity, creating a collide flow between steam and air around the exit. Under the condition with side channels, the cold air can be supplied to the cavity by means of four lateral entry streams, so its thermal dissipating power was greater than the case without side channels. The average temperature change between the sprinkling experiment with and without side flow channels is
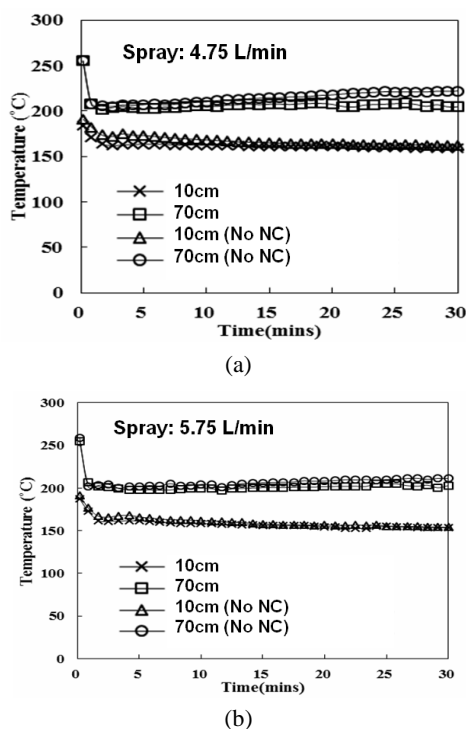
about 5% to 15%.

(a)

(b)

Fig. 14 Experimental temperature variations at water spray rate of (a) 4.75 l/min and (b) 5.75 l/min.

5 Conclusion

Though natural covection has limited capability in eliminating decayed heat, it is still a very effective cooling source when accident occurs. It extends the time of rescue to achieve partial elimination of decay heat. Sprinkling above the SPF into the pool can lower the zirconium-water reaction as a result of naked burning source. This research focuses mainly on the analysis and experiments in the cooling for SPF model. The conclusions of the research are illustrated as follow:

● Natural convection experiment points out that geometric change leads to a significant change by the effect of natural convection. The base flatboard height of 30cm has greater thermal efficiency than that of 10cm. As the space at the base of the flatboard is larger, the maximum amount of temperature decrease is about 55°C. In terms of the coefficients of different number of holes at the base of the flatboard, less amount of holes at the base leads to a decrease in the thermal dissipation capability. The maximum temperature difference

between the two different amount of holes is estimated to be 70 °C.

● Results between CFD simulations and experiments indicate a temperature difference of 7% to 25%, but the overall behavior is similar. This proves that CFD model can effectively capture the experiment phenomena. Therefore it is possible to use CFD model for further similar researches.

● In the simulations for different wattage of rod-bundle arrangement, both 2D and 3D models demonstrate that a pivotal speed in natrual convection is induced from higher power bundle with higher core temperature. Therefore, higher wattage bundle in the center pool could induce a higher efficiency in natural convection with a lower overall temperature.

● In 2D simulations, changing the base pool into a elevated geometric structure enhances the internal flow rate, thus increasing the efficiency of heat removal. But, the change in geometric shape of the base flatboard does not have an obvious effect in the natural convection.

● Different flow rate and individual sprinkling experiment prove that efficiency of natural convection will be increased when there is water sprinkling. During the course of the sprinkling experiment stream was continuously generated. Cool air can be supplied to enhance thermal dissipation around the exit of the natural convection. More spraying experiments have still been performing. Comparison would be made among different amounts of water being sprayed, different heights of spraying device, different time points of the water spraying in order to find out optimal suggestion.

Nomenclature

a_{net}	net absorption coefficient
c_p	constant-pressure specific heat
e	specific total energy
g	gravity
$I(r,\Omega)$	intensity of radiation at location of r in a direction Ω
$\tilde{I}$	unit tensor
K	inertial resistance factor
k	thermal conductivity
p	pressure

q_f	energy per unit fluid volume
$\vec{r}$	coordinate vector
S	source term
$\vec{S_i}$	force term per unit volume
T	temperature
$\vec{V}$	velocity = $u\vec{i} + v\vec{j} + w\vec{k}$

Greek symbols

ϕ	porosity
μ	dynamic viscosity
ρ	density
σ_s	scattering coefficient
Ω	coordinate direction vector

Subscript

b	black body
eff	effective
f	fluid
h	enthalpy
i	direction x, y or z
s	solid
t	turbulent

Acknowledgement

References

[1] ALVAREZ, R., BEYEA, J., JANBERG, K., KANG, J., LYMAN, E., MACFARLANE, A., THOMPSON, G., and HIPPEL, F.N.V.: Reducing the Hazards from Stored Spent Power-Reactor Fuel in the United States, Science & Global Security, 2003, 11:1-51.

[2] WANG, J. R., LIN, H. T., anf TSENG, Y. S.: Application of TRACE and CFD in the Spent Fuel of Chinshan Nuclear Power Plant, Appl. Mechanics & Materials, 2012, 145:78-82.

[3] WANG, J. R., LIN, H. T., LI, W. Y., CHEN, S. W., and SHIH, C.: Application of TRACE and FRAPTRAN in the Spent Fuel Pool of Chinshan Nuclear Power Plant, Appl. Mechanics & Materials, 2014, 479:543-547.

[4] DOGAN, M., SIVRIOGLU, M., and YILMAZ, O.: Numerical Analysis of Natural Convection and Radiation Heat Transfer from Various Shaped Thin Fin-Arrays Placed on a Horizontal Plate – a Conjugate Analysis, Energy Convers. Manage., 2014, 77:78-88.

[5] HUNG, T. C., and FU, C. S.: Conjugate Heat Transfer Analysis for the Passive Enhancement of Electronic Cooling through Geometric Modification in a Mixed Convection Domain, Numer. Heat Transfer, Part A, 1999, 35:519–535.

[6] YILMAZ, T., and FRASER, S. M.: Turbulent Natural Convection in a Vertical Parallel-Plate Channel with Asymmetric Heating, Int. J. Heat Mass Transfer, 2007, 50:2612-2623.

[7] NG, C. S., CHUNG, D., and DOI, A.: Turbulent Natural Convection Scaling in a Vertical Channel, Int. J. Heat & Fluid Flow, 2013, 44:554-562.

[8] TSENG, Y. S., WANG, J. R., TSAI, F. P., CHENG, Y. H., and SHIN, C.: Thermal Design Investigation of a New Tube-Type Dry-Storage System through CFD Simulations, Annuls of Nuclear Energy, 2011, 38:1088-1097.

[9] OFFICE OF NUCLEAR MATERIAL SAFETY AND SAFEGUARDS, Standard Review Plan for Dry Cask Storage Systems, U.S. NRC, NUREG-1536, 1997.

[10] LEE, D. S., LIU, M. L., HUNG, T. C., TSAI, C. H., and CHEN, Y. T.: Optimal Structural Analysis with the Associated Passive Heat Removal for AP1000 Shield Building, Appl. Thermal Eng., 2013, 50:207-216.

[11] YE, C., ZHENG, M. G., WANG, M. L., ZHANG, R. H., and XIONG, Z.Q.: The Design and Simulation of a New Spent Fuel Pool Passive Cooling System, Annuls of Nuclear Energy, 2013, 58:124-131.

[12] YOO, S. H., NO, H. C., KIM, H. M., and LEE, E. H.: CFD-Assisted Scaling Methodology and Thermal-Hydraulic Experiment for a Single Spent Fuel Assembly, Nucl. Eng. Des., 2010, 240:4008-4020.

[13] HUNG, T. C., DHIR, V. K., PEI, B. S., CHEN, Y. S., and TSAI, F. J.: The Development of a Three-Dimensional Transient CFD Model for Predicting Cooling Ability of Spent Fuel Pools, Appl. Therm. Eng., 2013, 50:496–504.

[14] YAN, Z. B., TOH, K. C., and DUAN, F.: Experimental Study of Impingment Spray Cooling for High Power Devices, Appl. Therm. Eng., 2010, 30:1225–1230.

[15] HOU, Y., LIU, X., LIU, J., LI, M., and PU, L.: Experimental Study on Phase Change Spray Cooling, Experi. Therm. & Fluid Sci., 2013, 46:84-88.

[16] JENSEN, P. K., LUND, I., and NUYTTENS, D.: Spray Liquid Distribution and Biological Efficiency of Commercially Available Nozzles Used for Precision Weed Control, Biosys. Eng., 2013, 116(4): 316-325.

[17] FRAKER, A. C.: Corrosion of Zrcaloy Spent Fuel Cladding in a Repository, US NRC, NISTIR 89-4114, 1989.

[18] INCROPERA, F. P., and DEWITT, D. P.: 1996, "Fundamentals of Heat and Mass Transfer-4th ed., Wiley, New York, 1996, page. 91.

[19] CHIU, E. H., and RAITHBY, G. D.: Computation of Radiant Heat Transfer on a Non-Orthogonal Mesh Using the Finite-Volume Method, Numer. Heat Transfer, PART B, 1993, 23:269-288.

[20] CHAI, J. C., LEE, H. S., and PATANKER, S. V.: Finite Volume Radiative Heat Transfer Procedure for Irregular

Geometries, AIAA J. Thermophys. Heat Transfer, 1995, 9(3):410-415.

[21] KIM, M. Y., and BAEK, S. W.: Numerical Analysis of Conduction, Convection, and Radiation in a Gradually Expanding Channel, Numer. Heat Transfer, PART A, 1996, 29(7):725-740.

[22] VANDOORMAAL, J. P., and RAITHBY, G. D.: Enhancement of the SIMPLE Method for Predicting Incompressible Fluid Flows, Numer. Heat Transfer, PART B, 1984, 7:147-163.

[23] RAITHBY, G. D., and CHUI, E. H.: A Finite-Volume Method for Predicting a Radiant Heat Transfer in Enclosures with Participating Media, Heat Transfer, 1990, 112:415-423.

[24] MURTHY, J. Y., and MATHUR, S. R.: A Finite Volume Method for Radiative Heat Transfer Using Unstructured Meshes, AIAA-98-0860, 1998.

[25] LAUNDER, B. E., SPALDING, D. B.: Lectures in Mathematical Models of Turbulence, Academic Press, London, England, 1972.

[26] TSAO, P. C., HSIEH, K. T., LEE, D. S., HUNG, T. C., TSENG, Y. S., and KIM, C. N.: Investigation of Passive Air Cooling Capacity for Spent Fuel Pool. In: 2013 World Congress on Advances in Nano, Biomechanics, Robotics, and Energy Research (ANBRE13), Seoul, Korea, 25 - 28 August, 2013.